J. Synchrotron Rad. (1996). **3**, 147–155

X-ray Optics of a Dynamical Sagittal-Focusing Monochromator on the GILDA Beamline at the ESRF

S. Pascarelli,[a]† F. Boscherini,[b]* F. D'Acapito,[c]† J. Hrdy,[d] C. Meneghini[b,e] and S. Mobilio[b,f]

[a]Istituto Nazionale per la Fisica della Materia, Via dell'Acciaio 139, I-16153 Genova, Italy, [b]Istituto Nazionale di Fisica Nucleare, Laboratori Nazionali di Frascati, PO Box 13, I-00044 Frascati (Roma), Italy, [c]Consiglio Nazionale delle Ricerche, P. le A. Moro 2, I-00182 Roma, Italy, [d]Institute of Physics, Czech Academy of Sciences, Na Slovance 2, 18040 Praha 8, Czech Republic, [e]Dipartimento di Fisica, Seconda Università di Roma, Via della Ricerca Scientifica 1, I-00133 Roma, Italy, and [f]Dipartimento di Fisica, Terza Università di Roma, Via della Vasca Navale 84, I-00146 Roma, Italy. E-mail: boscherini@lnf.infn.it

(*Received 26 December 1995; accepted 16 April 1996*)

The performance of a dynamical sagittal-focusing monochromator for hard X-rays is described. It consists of a flat first crystal and a diamond-shaped ribbed second crystal which is clamped by its central rib and dynamically bent by applying a force on its two apices. The system has proved to perform very well on the GILDA beamline at the ESRF. The horizontal acceptance varies with energy and with focusing geometry as predicted theoretically; the total available horizontal fan of radiation (3.6 mrad) is in fact collected in the 1:3 geometry. The system is routinely run in a dynamical focusing mode for XAFS spectroscopy in the energy range 5–30 keV with Si(311) crystals, with a constant spot size FWHM ~1 mm on the sample and without degradation of energy resolution or reproducibility. Using simple geometrical considerations we calculate the variations of the horizontal profile of the reflected beam during rocking-curve scans in different focusing geometries and find them in agreement with observed ones. Not only is this is a practical aid in alignment but it illustrates the X-ray optics of sagittal focusing in an elegant way.

Keywords: X-ray optics; dynamical diffraction; sagittal focusing; XAFS.

1. Introduction

Sagittal focusing with cylindrically bent crystals has been found to be an efficient method for focusing the diverging X-ray beam at synchrotron radiation sources (Sparks, Borie & Hastings, 1980; Sparks, Ice, Wong & Batterman, 1982). Several operational double-crystal $(n, -n)$ monochromators with a first flat crystal and a sagittally (cylindrically) bent second crystal have been developed (Matsushita, Ishikawa & Oyanagi, 1986; Heald & Sayers, 1989; Koyama *et al.*, 1992; Lamble & Heald, 1992; Stephens, Eng & Tse, 1993). The performance of such systems, in terms of horizontal acceptance and rocking-curve widths, is based on the evaluation of $\Delta\theta_\alpha$, the difference in incident angle between the first and the second crystal, as seen by a ray with horizontal deviation α from the central ray. In the general case $\Delta\theta_\alpha$ is an increasing function of α, with $\Delta\theta_\alpha = 0$ only for the central ray of the fan ($\alpha = 0$). When $\Delta\theta_\alpha$ exceeds the Darwin width the ray is not transmitted, limiting the horizontal width of the accepted radiation. In order to collect the whole horizontal fan of incident radiation, therefore, each divergent ray must meet the first and the second crystal at the same Bragg angle (to within the Darwin width), a condition which in the configuration flat crystal + cylindrically bent crystal is fulfilled only when the magnification M ($M = q/p$, where q and p are the distances between the bent crystal and the image and the source, respectively) is equal to 1/3 (Hrdy, 1994).

An improper alignment will contribute to increase this angular discrepancy and therefore reduce the transmission of the system. Misalignment between the axis of the cylinder and the axis of the incoming radiation (γ error), as well as a tilt of the second crystal around the latter axis (φ error), have to be corrected in order to have maximum throughput of horizontal divergence and theoretical rocking-curve widths (Koyama *et al.*, 1992).

Alignment is not always successful in the sense that often other factors interfere to hinder optimal transmission. These may originate from the crystals or from the bender. Sagittal bending introduces strain which tends to curve the crystal in the plane orthogonal both to the plane defined by the flat crystal and to that in which the sagittal bending occurs. This deformation (anticlastic curvature) limits the vertical acceptance of the system. An efficient method to reduce anticlastic bending is the stiffening of the crystal with ribs opposite the diffracting surface (Sparks *et al.*, 1982; Krisch, Freund, Marot & Zhang, 1991). Furthermore, improper bending and/or crystal clamping may cause a twist in the

† Mailing address: ESRF, GILDA CRG, BP 220, 38043 Grenoble CEDEX, France.

diffraction plane, disrupting the Bragg condition in whole portions of the surface. Finally, it is important to minimize strain due to crystal conditioning: thermal deformation and stress induced by mounting of the first crystal and strain related to machining or clamping on the second.

A very important issue that has to be considered when sagittal-focusing optics with bent crystals is used for X-ray-absorption fine-structure spectroscopy (XAFS) is the energy dependence of the focal distance. This effect is quite evident at low energies: using Si(311) crystals, a 1 keV energy scan at 6 keV causes a 25% variation in the focal distance, leading to a 10 mm increase in spot size in our system if an average radius of curvature is used. This problem, which is a major inconvenience for fluorescence XAFS and for transmission XAFS on small samples, can be overcome by changing the monochromator–sample distance to compensate the change in focal distance with energy (Heald & Sayers, 1989), or, in a more elegant and practical way, by changing the sagittal radius of curvature as a function of energy (Lamble & Heald, 1992). The success of the latter method is related to the ability of the bender to operate without inducing twist or other deformations on the surface of the crystal.

In this paper we describe the performance of a dynamically sagittally focusing monochromator, operational on the GILDA beamline at the ESRF (Pascarelli, Boscherini, Marcelli & Mobilio, 1992; Pascarelli *et al.*, 1995). This beamline, which accepts a 3.6 mrad horizontal fan from a 20 keV critical-energy bending magnet, is optimized to perform XAFS and powder diffraction in the energy range 5–50 keV with an energy resolution in the 10^{-5}–10^{-4} range, using Si(311) and Si(511) crystals. The system is based on a flat first crystal and a diamond-shaped ribbed second crystal, both diffracting in the vertical plane; the second crystal is clamped by its central rib and cylindrically bent by pushing on the two apices. A very simple bending device allows the radius of curvature to be decreased continuously during energy scans in order to keep the focal spot at a fixed distance. When properly clamped, this crystal is free from twist and easy to align.

We describe here a straightforward alignment procedure, based on the observation of the horizontal intensity distribution of the monochromatic reflection. Not only is this a practical aid in alignment but it shows the X-ray optics of sagittal focusing in a simple way. In §2 and §3 a brief overview of the sagittal-focusing principles and the alignment requirements are given. The crystal and the bender are described in §4. Finally, in §5 we report the performance of the system in terms of rocking-curve widths, accepted horizontal divergence, energy resolution and reproducibility.

2. Principles of sagittal focusing using Bragg diffraction from crystals

In order to obtain point-to-point focusing using Bragg reflecting crystals, two conditions have to be fulfilled: on the one hand, the reflecting planes must be curved to confocal ellipsoids of revolution with source and image at the foci (law of specular reflection), and on the other hand, the ellipsoids should be spaced so that the optical path between foci to any point on one ellipsoid differs from that to the adjacent ellipsoid by one wavelength (Bragg's law) (Berreman, Stamatoff & Kennedy, 1977). A good approximation to this ideal geometry is given by a cylindrical surface. Fig. 1(*a*) shows the optical path of rays leaving a point source S' with an arbitrary horizontal deviation from the central ray α, and which are focused in an image I through Bragg diffraction from a cylindrical crystal. The relation between Bragg angle θ_2, cylinder radius R_s, source-to-crystal distance p and crystal-to-image distance q can be obtained from the sagittal-focusing lens

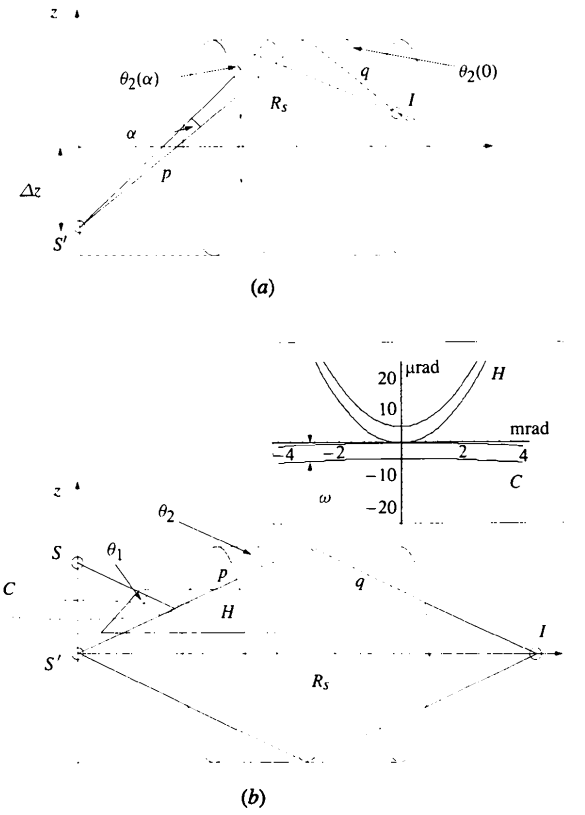

Figure 1
Schematic view of sagittal focusing using Bragg diffraction from a cylindrical crystal of radius R_s. p and q are the source-to-crystal and the crystal-to-image distances, respectively. As S' is moved from the axis of the cylinder ($\Delta z = 0$) to the surface of the cylinder ($\Delta z = R_s$), the magnification $M = q/p$ changes from a value of $M = 1$ to $M = 1/3$. (*a*) Optical system composed of one cylindrical crystal. Rays leaving the source S' with an arbitrary horizontal deviation α ($\alpha = 0$ corresponds to the axis of the cylinder) meet the surface of the cylinder with a Bragg angle θ_2 which is a function of α: $\theta_2 = \theta_2(\alpha)$. (*b*) Optical system composed of one flat crystal and one cylindrically bent crystal in a $(+n, -n)$ configuration. The $M = 1$ geometry case is illustrated. See text for a detailed explanation. In the inset we show the 'footprints' of rays transmitted from the first (footprint *C*) and from the second (footprint *H*) crystal, respectively, calculated for Si(311) crystals at 25 keV; x axis, horizontal divergence α (in mrad); y axis, angular deviation (in μrad).

equation:

$$1/p + 1/q = 2 \sin \theta_2/R_s. \quad (1)$$

The value of the magnification $M = q/p$ is easily seen to be related to the relative position of the source S' along the z axis:

$$M = 1/[1 + (2\Delta z/R_s)]. \quad (2)$$

As the source S' is moved from the axis of the cylinder ($\Delta z = 0$) to the surface of the cylinder ($\Delta z = R_s$), the magnification M changes from a value of $M = 1$ to $M = 1/3$. In the general case, rays leaving the source S' with an arbitrary horizontal deviation α meet the surface of the cylinder with a Bragg angle θ_2 which is a function of α: $\theta_2 = \theta_2(\alpha)$. The (monochromatic beam) horizontal acceptance of such a system is limited to a value α_{max} given by solving the following equation:

$$\theta_2(\alpha) - \theta_2(0) = \omega, \quad (3)$$

where ω is equal to the Darwin width of the crystal. However, Sparks *et al.* (1980) demonstrated the existence of a plane passing through an intermediate position Δz^* ($0 < \Delta z^* < R_s$) which intersects the cylinder at a constant θ_2. Therefore, a radiation fan emitted by a monochromatic source placed in Δz^* and belonging to this plane will be integrally transmitted. They showed that the value of M corresponding to this geometry is, for small Bragg angles, very close to 1/3.

Let us now consider our optical system, which is composed of a first flat and of a second cylindrically bent crystal. Its horizontal acceptance is limited to a value α_{max} given by the solution of the following equation:

$$\Delta\theta_\alpha = \theta_2(\alpha) - \theta_1 = \omega, \quad (4)$$

where θ_1 is the Bragg angle on the first crystal. A rocking-curve analogue is obtained by rocking one of the crystals through the 'parallelism' condition $\theta_1 = \theta_2(0)$. However, the shape and width of this curve are, in the general case, different from those relative to a flat-crystal's rocking curve, for which the profile is quasi-Gaussian and the width given by the convolution of the Darwin widths of the two crystals.

An elegant method has been proposed to illustrate the optics of sagittal focusing with a flat and a cylindrically bent crystal using simple geometrical considerations (Hrdy, 1992, 1994). It describes a straightforward way to calculate the horizontal acceptances, and shows that when $M = 1/3$ any ray diffracted by the first crystal will also be diffracted by the second one because $\theta_2(\alpha) = \theta_1$ (*i.e.* $\Delta\theta_\alpha$

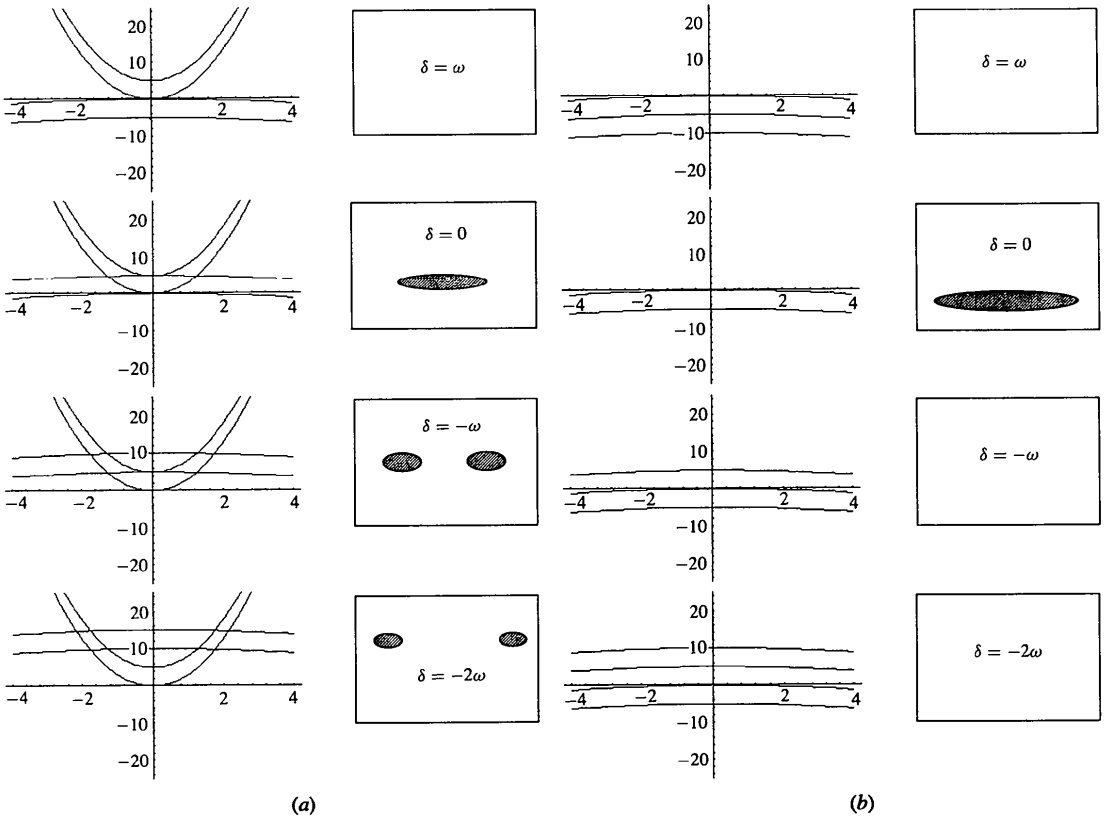

Figure 2
Rocking-curve scans in (*a*) the $M = 1$ geometry, and (*b*) the $M = 1/3$ geometry. See text for a detailed explanation. The curves have been calculated for Si(311) crystals at 25 keV. On the left-hand side of each panel we illustrate the result of calculations for successive values of δ from $\delta = +\omega$ to $\delta = -2\omega$, while on the right-hand side we show corresponding distributions of the reflection in a vertical plane between the second crystal and the image.

= 0) for all Bragg angles. A direct consequence of this is that rocking-curve profile and width in this geometry are identical to the configuration of the flat crystal. This method, for the simplest case corresponding to the M = 1 geometry, is summarized in Fig. 1(*b*). The circle C represents intersection points, on the plane of the first crystal, of rays from the source S, which are reflected from the first crystal with constant Bragg angle θ_1. The hyperbola H represents the intersection points on the first crystal of rays from the virtual source S' which impinge on the second crystal with a constant Bragg angle θ_2. The locus of these rays, which originate from the virtual source S' lying on the axis of the cylinder ($\Delta z = 0$), forms in fact a cone. To take into account the reflectivity functions of the crystals, the circle C and the hyperbola H have been replaced by corresponding 'footprints' of width equal to the Darwin width, ω. In the inset of Fig. 1(*b*) we show the 'footprints' which have been calculated for Si(311) crystals at 25 keV. Rays are transmitted by both crystals only if they belong to the intersection of the two 'footprints'. The situation is quite different in the 1:3 geometry. Here it can be shown that any ray from the virtual source S' (which now lies at $\Delta z = R_s$) forms exactly the same angle with the first (flat) crystal and with the second (cylindrical) crystal. In other words, all rays transmitted by the first crystal (*i.e.* reflected by the first crystal with Bragg angle θ_1) impinge on the second crystal with Bragg angle $\theta_2 = \theta_1$, being transmitted also by the second crystal. The two 'footprints' are therefore identical.

In Fig. 2 we illustrate the situation which occurs during a rocking-curve scan in the two geometries, the 1:1 and the 1:3. Curves in Fig. 2(*a*) refer to the 1:1 geometry and have been introduced in the inset of Fig. 1(*b*), while curves in Fig. 2(*b*) refer to the corresponding footprints in the 1:3 geometry. The curves have been calculated for Si(311) crystals at 25 keV. Let δ be the relative angle between the first and the second crystal: $\delta = \theta_1 - \theta_2(0)$. When δ is varied during a rocking-curve scan, the relative position of the footprints changes, as shown in Fig. 2. Also shown in Fig. 2 is the corresponding intensity distribution of the monochromatic reflection in a vertical plane placed between the second crystal and the image. In the 1:1 geometry, as δ is scanned through zero from positive to negative values, the central part of the horizontal fan appears first; it then gradually separates into two parts which drift further and further apart until they disappear at the corresponding α_{max} value. The two spots correspond to lateral parts of the second crystal successively meeting the Bragg condition at smaller Bragg angles with respect to the central part.* In the 1:3 geometry, on the other hand, a rocking-curve scan will give a monochromatic reflection which appears and disappears simultaneously on the whole width of the available acceptance, as illustrated in Fig. 2(*b*), analogous to what is observed in the rocking curve of a flat crystal. The experimental observation of the described features, related to the variations in the intensity of the reflected beam, constitutes the basis of an alignment criterion, as will be illustrated in the following section.

The intensity transmitted by the system as a function of δ, $I(\delta)$, is therefore proportional to the intersection area between the two footprints. The function $I(\delta)$ determines the shape and the width of the rocking curve. While the former is modified by the appearance of a 'tail' on the negative δ side whenever $M \neq 1/3$, the latter, ω_{tot}, may be estimated using the following convolution:

$$\omega_{tot} = (2\omega^2 + \Delta\theta_\alpha^2)^{1/2}. \qquad (5)$$

3. Alignment requirements for sagittal focusing

Other geometrical factors influence the horizontal acceptance of a double-crystal sagittal-focusing system. As shown in Fig. 3, besides the horizontal divergence relative to the central ray, α, and the Bragg angle, θ, two more angles are relevant: the misalignment between the axis of the cylinder and that of the incoming beam, γ, and the tilt of the second crystal around the 'correct' cylinder axis, φ.

The alignment procedure consists of reducing to a minimum the difference between the angles a horizontally diverging ray forms on the first crystal and on the second crystal. This quantity, indicated by $\Delta\Theta(\alpha,\gamma,\varphi)$, is given, to first order in γ and φ, by the sum of three quantities:*

$$\Delta\Theta(\alpha,\gamma,\varphi) = \Delta\theta_\alpha + \Delta\theta_\gamma + \Delta\theta_\varphi. \qquad (6)$$

* This formula has been obtained (Koyama *et al.*, 1992) for small α; however, the $\Delta\theta_\alpha$ contribution is identical to formulae found by Hrdy (1992, 1994) where no condition on α was defined. This suggests a more general validity of these formulae.

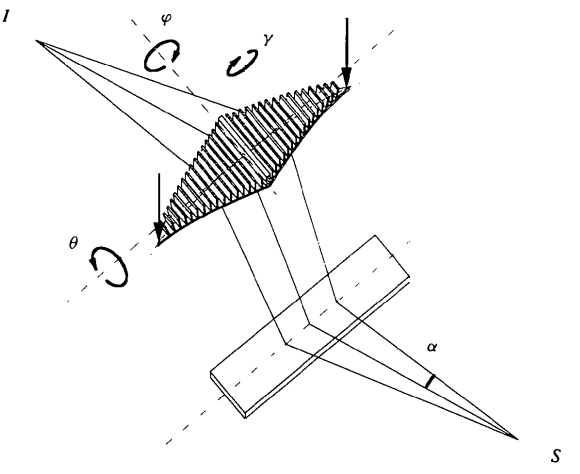

Figure 3
Schematic view of the optical system of the monochromator. The incident fan of radiation (3.6 mrad) is Bragg reflected by a first flat crystal and sagittally focused by a diamond-shaped ribbed second crystal which is cylindrically bent by applying a force on its two apices.

* An immediate application of the above considerations is that when crystal detuning is used to decrease harmonic content, it is advisable to detune using positive δ values whenever the experiment requires a homogeneous beam.

where:

$$\Delta\theta_\alpha = [4\sin(2\theta)]^{-1}[(1/M) + 1][3 - (1/M)]\alpha^2.$$

$$\Delta\theta_\gamma = (-2\sin\theta)^{-1}[(1/M) + 1]\gamma\alpha.$$

$$\Delta\theta_\varphi = (-2\cos\theta)^{-1}[(1/M) - 1]\varphi\alpha.$$

The relative importance of the three terms for typical values of γ and φ misalignment is illustrated with an example in Fig. 4: the three contributions are plotted as a function of horizontal deviation α for the 1:1 geometry at E = 25 keV. The first term $\Delta\theta_\alpha$ is quadratic in α and determines symmetrical horizontal intensity pattern variations during a rocking-curve scan, as shown in Fig. 2. As seen in the above section, $\Delta\theta_\alpha$ is unavoidable when $M \neq 1/3$, and poses the ultimate limit for acceptance. The second and third terms have a linear α dependence and determine asymmetric horizontal intensity pattern variations during a rocking-curve scan. These errors are eliminated in a perfectly aligned system. The importance of the $\Delta\theta_\gamma$ term has already been pointed out (Koyama *et al.*, 1992). This misalignment is easily detectable by observation of the distribution of the reflection after the second crystal during a rocking-curve scan, as it shifts horizontally when successive portions of the second crystal meet the Bragg condition. For $M \neq 1$, the α dependence of $\Delta\theta_\varphi$ is similar to that of $\Delta\theta_\gamma$ and can be aligned in the same way. It is worth noting that the α dependence for these two terms is similar, and one can, within limits, compensate a $\Delta\theta_\varphi$ misalignment with a corresponding $\Delta\theta_\gamma$ (and *vice versa*). As the terms $\Delta\theta_\varphi$ and $\Delta\theta_\gamma$ depend on the Bragg angle, optimization should in theory be made at each step of an energy scan, but in practice we have found that in a real energy scan this is not necessary as the variation in Bragg angle throughout a scan is not big enough to cause a detectable misalignment. To conclude, alignment can be considered successful when the horizontal intensity pattern of the monochromatic reflection viewed in a vertical plane between second crystal and image varies symmetrically during a rocking-curve scan, as illustrated in §2.

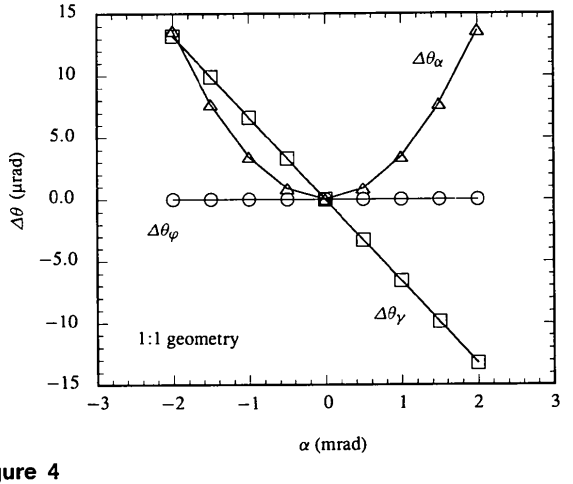

Figure 4
Contributions to the angular deviation between the first and the second crystal, as seen by a ray with horizontal deviation from the central ray α, due to horizontal divergence ($\Delta\theta_\alpha$), and to alignment errors ($\Delta\theta_\gamma$) and ($\Delta\theta_\varphi$). The calculation was performed using equation (6) for Si(311) crystals at E = 25 keV, in the M = 1 geometry. A value of γ = 1 mrad was used. The $\Delta\theta_\varphi$ term is absent (to first order in φ) in this geometry.

4. Description of the monochromator crystal and bender for dynamical sagittal focusing

The monochromator is composed of a first flat crystal and a second cylindrically bent crystal in the $(+n, -n)$ configuration. Bragg rotation θ is applied independently on the two crystals. Parallelism to within the μrad range is obtained using a closed feedback loop which acts on the first crystal through a piezo-actuator. The angle on the second crystal defines the energy through Bragg's law. This choice avoids energy calibration fluctuations due to temperature variations which are much weaker on the second crystal than on the first crystal, due to the high heat load induced by the incident beam. Constant height offset between the incoming white beam and the outgoing monochromatic beam as a function of Bragg angle θ is assured by translating the second crystal in the direction of the beam.

The first crystal is a 2 mm-thick flat rectangular plate in thermal contact with a water-cooled Cu block through an InGa eutectic. This cooling system is well adapted for the ESRF bending magnet beam, where the GILDA beamline is installed, the maximum incident power and absorbed power density (for a 0.2 A electron beam current) being of the order of 500 W and 1 W mm^{-2}, respectively.

As shown in Fig. 3, the second crystal has a diamond shape, with ribs opposite the diffraction surface. Rib height H, width W, and spacing S, and crystal thickness T, are of paramount importance in the optimization of a sagittal-focusing crystal because (*a*) the ratio R_s/R_a of the sagittal/anticlastic radii of curvature is a third-power function of T/H, with a weaker (linear) dependence on the ratio S/W (Sparks *et al.*, 1982), (*b*) the ultimate limit for the horizontal spot size is a function of W ($\Delta x \simeq 2W$ in a 1:1 geometry) (Sparks *et al.*, 1982), and (*c*) the ratio T/W strongly influences beam horizontal intensity homogeneity. In fact, as the crystal surface under the rib does not bend, the presence of the ribs induces inhomogeneities in the reflected beam related to periodic oscillations of the sagittal radius of curvature along the surface of the crystal. Numerical simulations using finite-element analysis have shown that an appropriate design of the ribs can reduce this effect considerably (Hazemann, Nayouf & de Bergevin, 1995). Our choice of rib design was driven by the very restrictive condition on the anticlastic curvature induced error, imposed by the extremely narrow rocking-curve widths of Si(311). Values of H/T = 20 and W = 1.2 mm were chosen. The central rib has a width equal to $2W$. The focal dimensions we obtain, FWHM $\simeq$1 mm, are compatible with this value of W. The importance of a central thick rib is twofold: it helps to limit anticlastic

curvature and it makes the crystal less sensitive to clamping strain.

The second crystal is clamped by its central rib to a holder which is then inserted in the bender (Fig. 5). The crystal holder can be easily extracted allowing a change of crystals to be performed without major intervention. The bender is situated in an inner cradle which is free to γ-rotate in an outer cradle on which Bragg-angle rotation θ is applied. The bending is performed by simultaneously pushing the two apices of the crystal. The choice of the shape was mainly based on considerations regarding the minimization of stress and twist induced by the clamping and bending methods. On this basis, an isosceles triangular crystal clamped on its short side would have been the best choice but it was excluded due to the vertical and horizontal shifts of the focal spot with energy. As the crystal is 280 mm wide whereas the beam footprint on the crystal is only 100 mm, the action of the pushers is far from the diffracting region. Local surface distortions which are present in the proximity of the pushers are therefore far from the illuminated region. Moreover, the fact that the bending force is applied on two points instead of on lines parallel to the cylinder axis (as in rectangular-shaped crystals) minimizes twist induced by the bender. The two pushers are activated by a single direct-current motor through a system of mechanical lever arms. An optical encoder (resolution = 0.5 μm, accuracy ~1 μm) keeps track of the elongation of the motor axis. The measured relative position error between the two pushers is equal to 10 μm. Values of sagittal radii of curvature used range between 1 and 13 m, yielding a maximum pusher elongation of *ca* 4 mm.

5. Performance

We shall first describe the sagittal-focusing properties of the monochromator, and then review its overall performance in terms of rocking-curve widths, horizontal acceptance, resolution and reproducibility. When the system is properly aligned the predicted symmetric variations in the horizontal distribution of the intensity of the reflected beam can be observed. The image formed on a fluorescent screen placed immediately after the monochromator changes in the manner shown in Fig. 2 as the first crystal is rotated through the Bragg angle, for the 1:1 and the 1:3 geometry, respectively. In Figs. 6(*a*) and 6(*b*) we report photographs of the beam for the 1:1 and the 1:3 geometries, respectively. The fluorescent screen was placed at a distance from the focal spot equal to $0.95q$ and $0.85q$ for the 1:1 and the 1:3 geometries, respectively. If the total 3.6 mrad fan were to be transmitted simultaneously, the width of the reflection would be equal to 95 and 85 mm in the 1:1 and 1:3 geometries, respectively. As shown in the series of photographs, in the 1:1 geometry the reflection appears in the centre and gradually separates into two spots which drift further and further away from each other. In the 1:3 geometry, however, the total width is illuminated simultaneously. The observed features are not only a practical aid in alignment, but nicely illustrate the optics of X-ray sagittal focusing.

Fig. 7 shows rocking curves at E = 25 keV, measured at maximum power and with vertical and horizontal divergences $\simeq$ 30 μrad and 3.6 mrad, respectively, in the two geometries discussed above. The curve recorded in the 1:3 geometry has, as expected, a Gaussian profile, while in the 1:1 geometry the shape is distorted as predicted from theory, with a negative tail corresponding to the lateral parts of the second crystal meeting the Bragg condition at smaller Bragg angles with respect to the central part of the crystal. The measured FWHM of the curve relative to the 1:3 geometry is $\omega_{tot}(1{:}3) \simeq 10$ μrad. The observed discrepancy between this value and the theoretical flat-crystal's rocking-

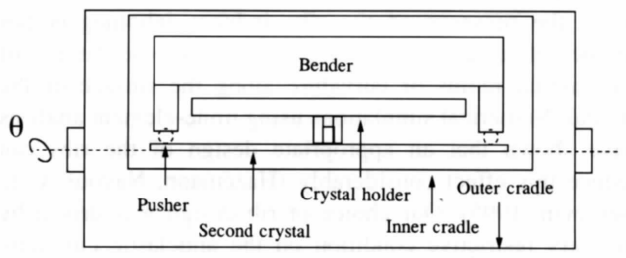

Figure 5
Schematic drawing of the bender for dynamical sagittal focusing of the monochromator. The second crystal is clamped by its central rib and cylindrically bent by applying a force on its apices. The remaining ribs are not shown for clarity. The crystal holder is inserted into an inner cradle and can be removed without major interventions.

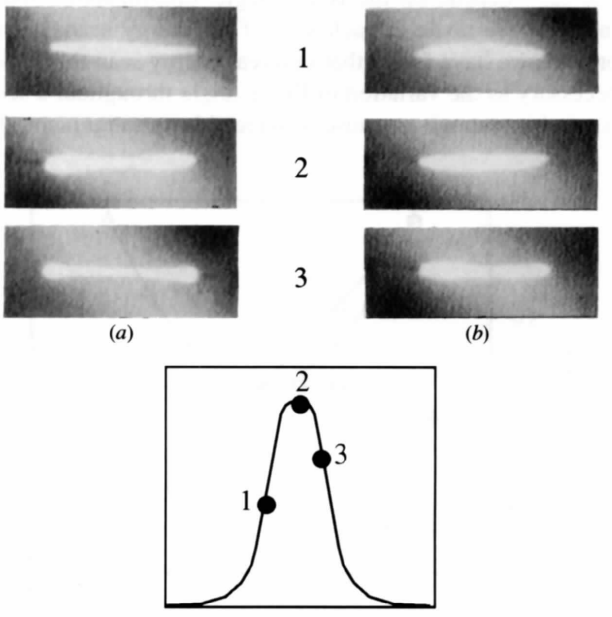

Figure 6
Sequence of photographs of the monochromatic reflection at three different alignments of the two crystals: (*a*) in the M = 1 geometry, and (*b*) in the M = 1/3 geometry. The inset shows the corresponding points on the rocking curve at which the photographs were taken. In the 1:1 geometry the reflection appears at the centre of the image and gradually separates into two spots which drift further and further apart, while in the 1:3 geometry the whole width of the image appears and disappears simultaneously.

curve FWHM, which at 25 keV with Si(311) crystals is $2^{1/2}\omega \simeq 6$ μrad, is, we believe, due to the presence of a small amount of strain on the first crystal. From our experience, the thin eutectic layer which improves thermal contact at the Si/Cu interface has a negative side effect of introducing a small $\omega_{strain} \simeq 7$ μrad. The experimental evidence supporting this hypothesis is (*a*) the measured FWHMs start deviating from theoretical values only at high energies, and (*b*) rocking-curve widths measured using different second-crystal configurations (flat unribbed, flat ribbed, bent 1:3 configuration) are identical.

From the measured FWHM of the rocking curve in the 1:1 configuration, which is $\omega_{tot}(1{:}1) \simeq 14$ μrad, and from the estimated FWHM contribution due to strain, we may predict the value of $\Delta\theta_{\alpha(exp)}$ using equation (5): $\Delta\theta^2_{\alpha(exp)} = \omega^2_{tot}(1{:}1) - \omega^2_{tot}(1{:}3) = \omega^2_{tot}(1{:}1) - 2\omega^2 - \omega^2_{strain}$. The value obtained in this way is $\Delta\theta_{\alpha(exp)} \simeq 10.5$ μrad. This value compares well with the predicted theoretical value $\Delta\theta_{\alpha(th)} = 10.8$ μrad obtained from equation (6) at 25 keV in the 1:1 geometry and with a total incident horizontal fan of 3.6 mrad ($\alpha = 1.8$ mrad).

The horizontal acceptance of the system with Si(311) crystals has been estimated at different energies in the 1:1 and the 1:3 geometries by comparing the maximum intensity of a rocking curve recorded with the curved crystal $I_{foc}(0)$ to the maximum intensity obtained when the crystal is flat $I_{flat}(0)$. Measurements have been performed at maximum power and with vertical and horizontal divergences of ~30 μrad and 3.6 mrad, respectively. The intensity profiles as a function of δ, $I(\delta)$, have been measured by rotating the first crystal around the Bragg angle (40 μrad $\leq \delta \leq$ −40 μrad), and recording the transmission of the system using an ionization chamber placed immediately after the monochromator which collects the total divergence. In Fig. 8 we plot the effective number of mrad that are transmitted by the system as a function of energy for the two geometries. This number has been obtained by normalizing the ratio $I_{foc}(0)/I_{flat}(0)$ to the number of incident mrad. Theoretical curves obtained from equation (4) have also been plotted for comparison. The overall comparison is good, with only a small decrease in the maximum of the intensity of the rocking curves at high energy for M = 1/3, which is consistent with the observed enlargement of the rocking curves. The effective gain in photon density on the sample has been established by verifying that all the photons measured by the first ionization chamber are effectively collected through a 2 mm slit placed in the sample position.

The performance of the optics in terms of rocking-curve widths and horizontal acceptance compares well with theoretical predictions, making this system not only practical (easy to align, quick access to crystals, *etc*) but also very efficient and accurate.

The dynamically focusing mode has been successfully used at all energies covered by the Si(311) crystals for X-ray absorption spectroscopy in the transmission and fluorescence modes. We would like here to underline the fact that having a focused spot which does not change shape or position throughout energy scans is not only essential for fluorescence measurements (for obvious solid-angle variation effects), but is very important also in transmission measurements on 'real' samples, as signal-to-noise ratios relative to non-ideal samples have improved considerably. Therefore, we have found that this mode of operation has advantages that go well beyond a mere gain in photon density on the sample. In fact, in the great majority of measurements performed in the transmission mode, we find that having a constant spot size on the sample during the energy scan is by far more important than having a gain in the number of photons on the sample due to

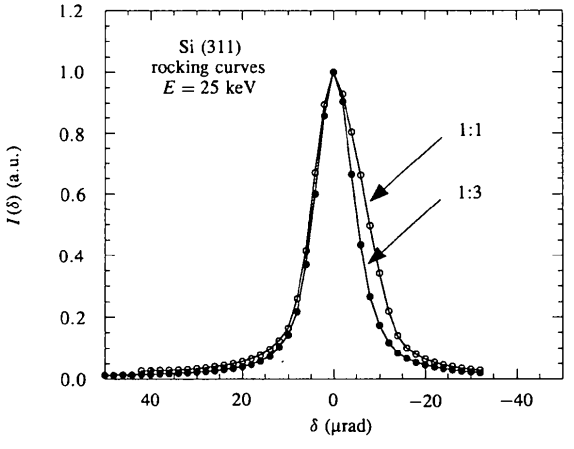

Figure 7
Comparison between rocking curves registered in the M = 1 geometry and in the M = 1/3 geometry. Normalized transmitted intensity $I(\delta)$ is plotted as a function of angular deviation δ. The curves have been registered using Si(311) crystals at 25 keV using the maximum horizontal fan of radiation (2α = 3.6 mrad). As expected from theory, the curve relative to the 1:1 geometry is asymmetric, showing a 'tail' for negative values of δ. The increase in the measured FWHM yields $\Delta\theta_\alpha$ = 10.5 μrad, which is consistent with the expected value of $\Delta\theta_\alpha$ = 10.8 μrad obtained from equation (6).

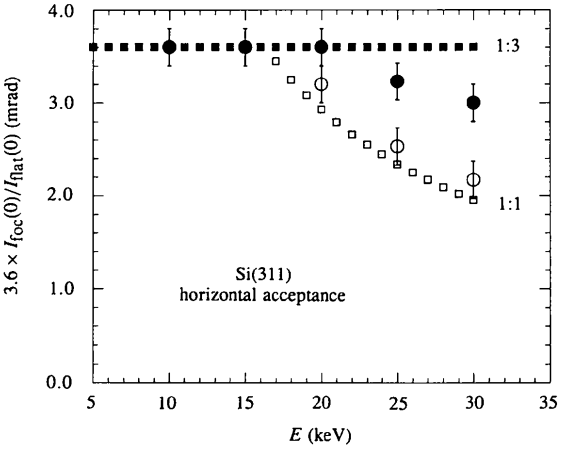

Figure 8
Horizontal acceptance (number of mrad effectively transmitted) of the optical system as a function of energy for the M = 1 (empty symbols) and M = 1/3 (filled symbols) geometries. The circles indicate experimental estimates (see text) while the squares indicate theoretical values calculated using equation (4).

the sagittal focusing. On the other hand, measurements in the fluorescence mode benefit both from a gain in photon density on the sample and from a constant spot size.

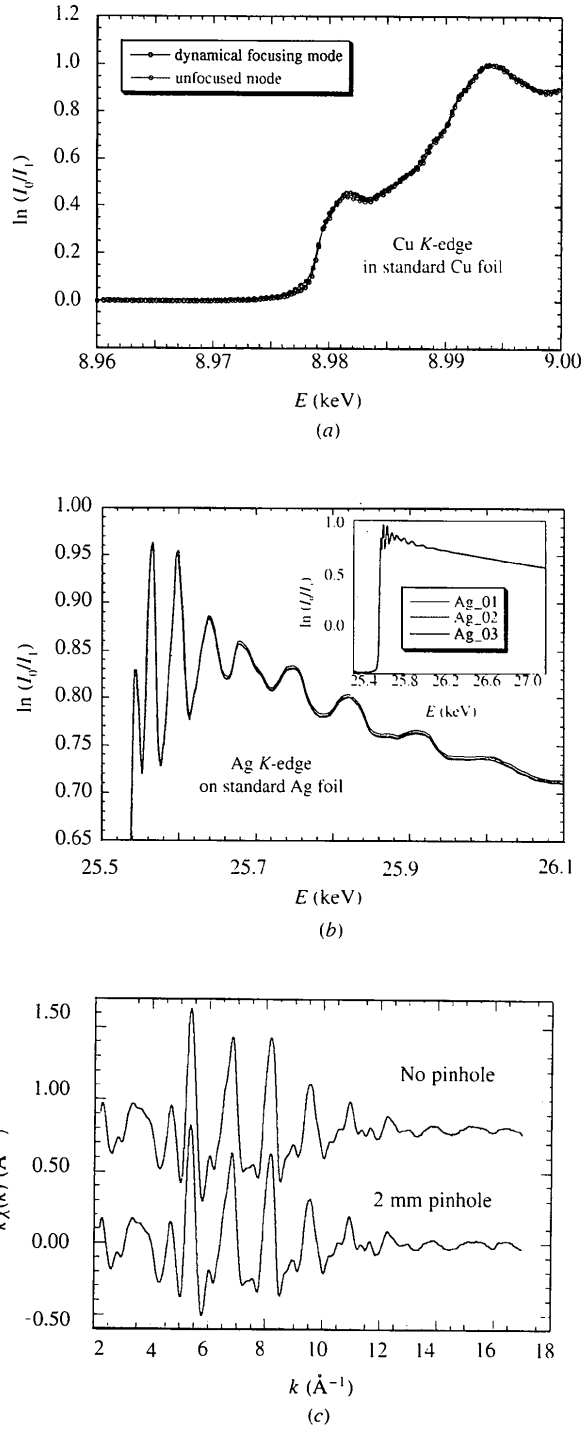

Figure 9
Tests on resolution and global system reproducibility: (*a*) Near-edge absorption spectra of Cu foil, registered in a dynamical focusing mode and in an unfocused (flat crystal) mode. Energy resolution is not affected, as all edge structures are reproduced without distortion. (*b*) Three superimposed XAFS spectra of an Ag foil, measured in a dynamical focusing mode, showing high reproducibility. (*c*) Two XAFS spectra of an Fe foil measured in dynamical focusing mode, with and without a 2 mm square pinhole at the sample position: no differences are found.

Finally, we have performed a number of tests to check for the presence of unwanted effects related to the dynamical focusing operation mode and to establish the overall reproducibility of the mechanics of the monochromator. In particular, as it is the second crystal which defines the energy at each step during the scan, it was important to exclude energy calibration loss during the spectra due to unwanted distortions of the crystal surface caused by the continuous variation of the radius of curvature. This would appear as a loss of resolution with respect to a 'flat-crystal' or a 'fixed-radius' mode of operation. We have observed no appreciable increase in the monochromator dead time during energy scans, caused by the dynamical focusing mode. All the X-ray absorption measurements have been performed using ionization chambers to record the photon intensity before (I_0) and after transmission by the sample (I_1), in the standard geometry. In Fig. 9(*a*) we compare a near-edge spectrum of a Cu foil registered in a dynamically focusing mode with one registered without bending the second crystal. The two spectra are identical so we conclude that energy resolution is not affected by sagittal focusing, nor are any distortions introduced. A reproducibility test is illustrated in Fig. 9(*b*) where we show three superimposed *K*-edge extended absorption spectra of a standard Ag foil. The extremely high degree of reproducibility is obtained through the coupling of good mechanics with the high beam stability offered by the ESRF storage ring. Finally, in Fig. 9(*c*) we compare two transmission XAFS spectra of a standard Fe foil performed with dynamical focusing with and without a 2 mm square pinhole placed at the sample position; no differences are noticeable in signal-to-noise ratio nor are any distortions introduced by the presence of the pinhole. We conclude that the bender is able to keep a constant spot size (FWHM ~1 mm), at the same position, throughout the XAFS scan. We stress that at the Fe edge with Si(311) crystals the variation of radius of curvature during a scan is particularly large; in fact, if a fixed average radius of curvature is used the horizontal spot size will reach a maximum of 10 mm. Therefore, this is a particularly stringent test of the bender. Identical results are obtained at all energies.

Note added in proof: Since submitting the manuscript we have been successful in obtaining dynamical sagittal focusing with Si(511) crystals.

It is a pleasure to acknowledge A. Savoia for his contribution to the design of the monochromator in the initial phase. Partial support by the Commission of the European Communities (in the form a research fellowship to JH) is acknowledged. We are grateful to F. Comin and to A. Freund for useful discussions. The bender was manufactured by Viglietti Meccanica, 17014 Cairo Montenotte (SV), Italy. The crystals were machined by A. Paul. We are indebted to F. Campolungo, L. Sangiorgio, V. Sciarra and V. Tullio for excellent technical assistance.

References

Berreman, D. W., Stamatoff, J. & Kennedy, S. J. (1977). *Appl. Opt.* **16**, 2081–2085.

Hazemann, J. L., Nayouf, K. & de Bergevin, F. (1995). *Nucl. Instrum. Methods*, **B97**, 547–550.

Heald, S. M. & Sayers, D. E. (1989). *Rev. Sci. Instrum.* **60**, 1932–1935.

Hrdy, J. (1992). *Rev. Sci. Instrum.* **63**, 914–915.

Hrdy, J. (1994). *Rev. Sci. Instrum.* **65**, 2147–2148.

Koyama, A., Nomura, M., Kawata, H., Iwazumi, T., Sato, M. & Matsushita, T. (1992). *Rev. Sci. Instrum.* **63**, 916–919.

Krisch, M., Freund, A., Marot, G. & Zhang, L. (1991). *Nucl. Instrum. Methods*, **A308**, 378–380.

Lamble, G. M. & Heald, S. M. (1992). *Rev. Sci. Instrum.* **63**, 880–884.

Matsushita, T., Ishikawa, T. & Oyanagi, H. (1986). *Nucl. Instrum. Methods*, **A246**, 377–379.

Pascarelli, S., Boscherini, F., Marcelli, A. & Mobilio, S. (1992). *Rev. Sci. Instrum.* **63**, 927–930.

Pascarelli, S., D'Acapito, F., Antonioli, G., Balerna, A., Boscherini, F., Cimino, R., Dalba, G., Fornasini, P., Licheri, G., Meneghini, C., Rocca, F. & Mobilio, S. (1995). *ESRF Newsl.* **23**, 17–19.

Sparks, C. J. Jr, Borie, B. S. & Hastings, J. B. (1980). *Nucl. Instrum. Methods*, **172**, 237–242.

Sparks, C. J. Jr, Ice, G., Wong, J. & Batterman, B. (1982). *Nucl. Instrum. Methods*, **194**, 73–78.

Stephens, P. W., Eng, P. J. & Tse, T. (1993). *Rev. Sci. Instrum.* **64**, 374–378.